Magnetic stability under magnetic cycling of MgO-based magnetic tunneling junctions with an exchange-biased synthetic antiferromagnetic pinned layer

Cite as: AIP Advances **6**, 025303 (2016); https://doi.org/10.1063/1.4941753
Submitted: 16 July 2015 • Accepted: 27 January 2016 • Published Online: 05 February 2016

Qiang Hao, Cameron Reid, Gang Xiao, et al.

Magnetic stability under magnetic cycling of MgO-based magnetic tunneling junctions with an exchange-biased synthetic antiferromagnetic pinned layer

Qiang Hao,[1] Cameron Reid,[1] Gang Xiao,[1,a] and Hon Ming Chan[2]
[1]*Physics Department, Brown University, Providence, Rhode Island 02912, USA*
[2]*Department of Physics, The Chinese University of Hong Kong, Shatin, Hong Kong, China*

(Received 16 July 2015; accepted 27 January 2016; published online 5 February 2016)

We investigate the magnetic stability and endurance of MgO-based magnetic tunnel junctions (MTJs) with an exchange-biased synthetic antiferromagnetic (SAF) pinned layer. When a uniaxially cycling switching field is applied along the easy axis of the free magnetic layer, the magnetoresistance varies only by 1.7% logarithmically with the number of cycles, while no such change appears in the case of a rotating field. This observation is consistent with the effect of the formation and motion of domain walls in the free layer, which create significant stray fields within the pinned hard layer. Unlike in previous studies, the decay we observed only occurs during the first few starting cycles (<20), at which point there is no further variance in all performance parameters up to 10^7 cycles. Exchange-biased SAF structure is ideally suited for solid-state magnetic sensors and magnetic memory devices. [http://dx.doi.org/10.1063/1.4941753]

A simple model of a magnetic tunneling junction (MTJ) includes three key layers from top to bottom: a soft ferromagnetic layer (free layer), an insulator, and a hard ferromagnetic layer (hard layer).[1–4] The magnetization of the hard layer is fixed with its direction serving as a reference axis, even under the constant agitation of external magnetic fields. The magnetization direction of the free layer is along an in-plane easy axis. In zero field, if this easy axis is perpendicular to the reference axis, the MTJ serves as a magnetic sensor device.[5] On the other hand, if parallel, the MTJ behaves as a non-volatile magnetic memory cell.[6,7] In both types of devices, the magnetization of the free layer constantly changes its direction from small to large angles (180°). For sensors, the magnetic endurance should be at least a few million cycles. However, for magnetic random access memories (MRAMs),[6,7] 10^{15} cycles are required for a 10-year usage. The magnetic stability of MTJ devices is therefore critically important for the accuracy of magnetic sensing and the retention of long-term memory states.

Experimentally, it has been found that,[8] after 10^7 cycles of uniaxial switching of the free layer in simple MTJs of $Co_{75}Pt_{12}Cr_{13}/Al_2O_3/Ni_{40}Fe_{60}$ or Co, complete logarithmic demagnetization occurs in the hard layer ($Co_{75}Pt_{12}Cr_{13}$) even though the external field is much smaller than the switching field of the hard layer. The magnetic instability was attributed to the demagnetizing influence on the hard layer of the strong stray fields generated by the domain walls within the free layer during magnetization reversal.[9–11] Exchange-biasing the hard layer (MnFe/Co) was found to substantially improve the stability of the hard layer.[8] However, significant magnetic decay was still observed using an antiferromagnetically coupled hard layer (Co/Cu/Co).[12] The interlayer magnetostatic coupling is a key parameter in the performance of MTJs.[13,14] Magnetic stability in coupled magnetic structures has received much attention in recent years due to the promising potential of spintronics.[7–19]

Applications of MTJs have extended beyond read heads in hard disk drives and MRAMs. MTJ sensors have been used for medical and biological devices,[20,21] scanning magnetic microscopes,[22,23]

[a]Electronic mail: Gang_Xiao@Brown.edu

high frequency oscillators,[24] non-destructive testing,[25] current sensors,[26] and ultra-low noise sensors.[27] MTJ sensors due to its high sensitivity and thermal performance have becoming an enabling technology in many areas of science and engineering. However, many challenges remain. In order to sense small changes in magnetic field under a wide field dynamic range, the magnetic stability of the MTJs is an important issue. High stability is most beneficial to long life time and accuracy of the MTJ magnetic sensors. Another issue is the intrinsic magnetic noise of the MTJ sensors. Lower noises will extend the applications to areas where traditional Hall or anisotropic magnetoresistive (AMR) sensors are ineffective. Better magnetic stability also leads to lower magnetic noise.

In this work, we study the magnetic stability of MgO-based MTJs under a large number of magnetic cycling. We use a realistic layer structure commonly used in commercial MTJ sensors[5] and MRAMs. In particular, the hard layer consists of an exchange-biased synthetic antiferromagnetic (SAF) pinned layer, which is considered as a more stable magnetic structure than a simple hard magnet or exchange-biased magnet. We report extremely high magnetic stability after 10^7 cycles of either linear switching or coherent rotation. The finding bodes well for spintronics applications that require long-term endurance.

Our MTJ multilayer stacks are deposited on thermally oxidized silicon substrates using a custom high vacuum magnetron sputtering system with a base pressure of 2×10^{-8} Torr. The MTJs have the following structure (thicknesses in nm): substrate/Ta(5)/Ru(30)/Ta(5)/$Co_{50}Fe_{50}$(2)/IrMn(15)/$Co_{50}Fe_{50}$(2)/ Ru(0.8)/$Co_{40}Fe_{40}B_{20}$(3)/MgO(2)/$Co_{40}Fe_{40}B_{20}$(3)/contact layer. The IrMn(15)/$Co_{50}Fe_{50}$(2)/Ru(0.8)/$Co_{40}Fe_{40}B_{20}$(3) layer assembly just below the MgO barrier is the SAF pinned layer. The net magnetization vector of the SAF layer is fixed in the plane of the layer, and only weakly perturbed by an external field. The CoFeB layer above the MgO barrier is patterned into an oval shape with a certain aspect ratio. All layers except for the MgO layer were deposited by DC magnetron sputtering at a constant Ar pressure of 1.5 mTorr. The MgO layer was deposited by radio frequency (RF) magnetron sputtering at an Ar pressure of 1.1 mTorr. During deposition, the wafers rotate at about 50 RPM to ensure thickness uniformity of the multilayer structure. Junctions were patterned using standard optical lithography and ion milling procedures. Each MTJ sample consists of 38 elliptical junctions connected in series. The individual MTJ element has an oval shape with 50 μm and 90 μm as the lengths of the two major axes (*i.e.*, aspect ratio of 1.8). The 38 MTJ elements are placed within an area of 890×890 μm^2. The pitch is 170 μm. The series arrangement of the MTJ elements is to increase the immunity against the electrostatic discharge (ESD) of the individual MTJ element. At zero field, typical resistance of the MTJ sensor is about 0.6 to 6 kΩ with a RA (Resistance Area) of 56-560 kΩ-μm^2. The device biasing field at zero field is 0.5 V. As a final step of fabrication, we perform magnetic thermal annealing in a vacuum chamber ($\sim 1 \times 10^{-6}$ Torr) on the MTJ sensors to define the pinning axis for the bottom magnetic electrode. A uniform magnetic field of 0.45 T is applied in the plane of the MTJ multilayer. Annealing occurs at 310 °C for 4 h with natural cooling. For the samples used in this study, the magnetic easy axis which is along the long major axis of the ellipse is aligned along the pinning direction of the pinned magnetic layer. This is generally referred to as the magnetic memory configuration.

In order to study the magnetic stability of the MTJs, the samples are subjected to an external in-plane oscillating sinusoidal magnetic field with an amplitude of 100 Oe and a frequency of 50 Hz along the easy axis of the free layer (uniaxial switching mode) or a rotating magnetic field with a constant amplitude of 100 Oe and a frequency of 100 Hz (coherent rotation mode). In either method, the maximum applied field is sufficient to saturate the magnetization of the free layer, while too small to have any direct influence on the magnetization state of the pinned layer. After a certain number (N) of cycles, we measure the magnetic transfer curve of the MTJ sample, i.e., the tunneling resistance as a function of a linearly sweeping magnetic field from +100 Oe to -100 Oe and back to +100 Oe, applied along the easy axis of the free layer. All of our measurements are carried out at room temperature.

Figure 1 shows such a magnetic transfer curve of a representative MTJ sample (MTJ-1). Within the field range of ±100 Oe, the magnetoresistance response is primarily from the free layer of 3-nm $Co_{40}Fe_{40}B_{20}$. In our MTJ samples, the exchange-bias provides a pinning field of about 500 Oe for the SAF hard layer, which remains mostly inert within ±100 Oe. Based on the transfer curves, we obtain the magnetic coercivity $H_c(N)$ as a function of cycling number N for the free

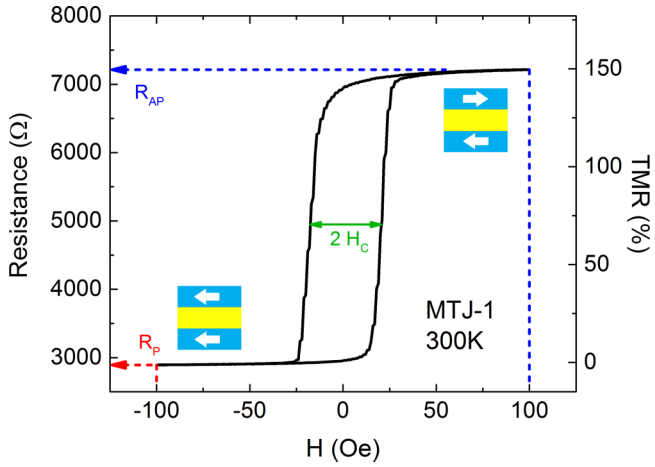

FIG. 1. Tunneling magnetoresistance transfer curve for an MTJ sample (MTJ-1) within the magnetic field range of ±100 Oe. R_{AP} and R_P are the resistance values at +100 Oe and -100 Oe, respectively, corresponding to the anti-parallel and parallel magnetization states between the free layer and the hard layer. The TMR value is in reference to R_P. Coercivity H_C is the half width of the loop at the mid-section of the transfer curve.

layer as shown in Fig. 1. The parallel resistance $R_P(N)$ and the antiparallel resistance $R_{AP}(N)$ correspond to the resistances of the parallel and antiparallel magnetization alignment, respectively, between the free and the hard layer. The tunneling magnetoresistance ratio TMR(N) is defined as $[R_{AP}(N)\text{-}R_P(N)]/R_P(N)$. The TMR is above 100% for our samples, and 150% for MTJ-1 used in Fig. 1.

We use 4 MTJ samples, with 2 for endurance test in uniaxial switching mode and another 2 for coherent rotation mode. Figure 2 shows coercivity $H_c(N)$ versus cycling number N in the range of 1 to 10^7 which lasts a couple of days. Within an experimental error of about 0.5%, $H_c(N)$ remains constant for both cycling modes. This observation indicates that the free layer retains its

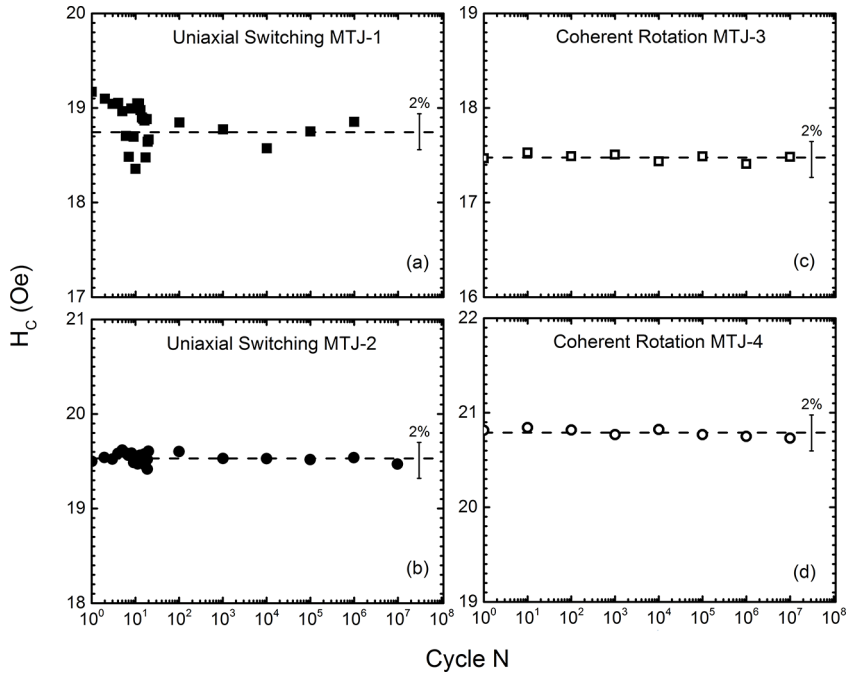

FIG. 2. Coercivities H_C of the free layer as functions of magnetic cycling number N for sample MTJ-1 (a) and MTJ-2 (b) undergoing uniaxial magnetic switching, and for sample MTJ-3 (c) and MTJ-4 (d) undergoing coherent rotation.

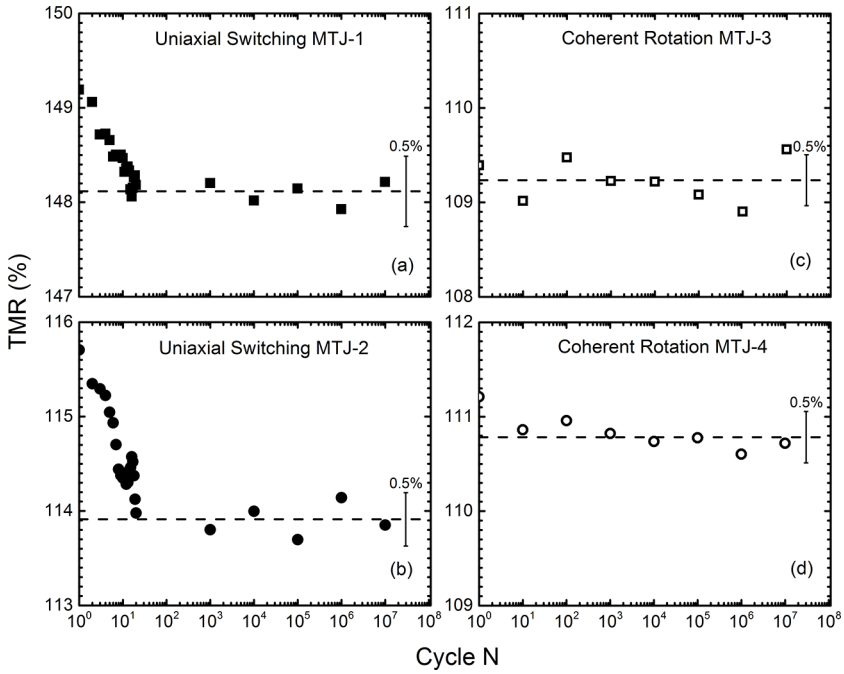

FIG. 3. TMR values as functions of magnetic cycling number N for sample MTJ-1 (a) and MTJ-2 (b) undergoing uniaxial magnetic switching, and for sample MTJ-3 (c) and MTJ-4 (d) undergoing coherent rotation.

magnetic property and is able to endure magnetic agitations up to ±100 Oe. It is noted that $H_c(N)$ is an important parameter for MRAMs and magnetic sensors. Variation in H_c will affect magnetic writing accuracy in MRAMs, and magnetic sensitivity and calibration in magnetic sensors. The low variance in H_c observed in Fig. 2 is assuring for spintronics applications.

Figure 3 shows the TMR variance versus cycling N. Under uniaxial switching, the TMR value decreases by 0.74% and 1.62% for two individual samples (MTJ-1 and MTJ-2) logarithmically during the first 20 cycles (the "training period"). Thereafter, TMR remains constant within our experimental error (0.3%) up to our maximum 10^7 cycles. The observed long-term magnetic stability is superior to what are reported in similar studies[8,12,15,19] which use different magnetic layer structures from ours. Furthermore, as shown in Fig. 3, the coherent rotation mode results in no variance in TMR value at all (within experimental error) for samples MTJ-3 and MTJ-4, over both short-term and long-term endurance tests (N from 1 to 10^7).

The initial decrease in TMR under uniaxial switching during the "training period" is small, but real, and can be caused by either $R_{AP}(N)$ or $R_P(N)$ or both. Figure 4 shows the variations of $R_{AP}(N)$ and $R_P(N)$ versus cycling number N. In the uniaxial switching mode, $R_{AP}(N)$ decreases, but $R_P(N)$ increases logarithmically during the "training period". Afterwards, both stay constant up to 10^7 cycles. As expected, both $R_{AP}(N)$ and $R_P(N)$ remain constant over the whole endurance test in the coherent rotation mode.

There are two major differences between our work and earlier work.[8,9] Earlier, the hard magnetic electrode is a simple hard layer, whereas our hard layer consists of an exchange-biased synthetic antiferromagnetic pinned layer. Secondly, the simple hard layer becomes demagnetized (90% reduction in magnetization) after 10^5 to 10^7 magnetic cyclings.[8,9] In our SAF, magnetic stability persists to our maximum 10^7 cyclings with negligible magnetic decay.

It is generally accepted that any magnetic instability is not caused by the magnetic integrity of the free layer.[8–12,17,19] In our measurement, we find that the magnetic properties, particularly H_C, are not affected by either uniaxial switching or coherent rotation. However, any magnetic inhomogeneity such as domain walls in the free layer would create very large stray fields within the hard layer located just a couple of nanometers away from the free layer.[8–11,17] These stray fields become dynamic abruptly during uniaxial switching.[8–11] Through interlayer dipolar couplings,

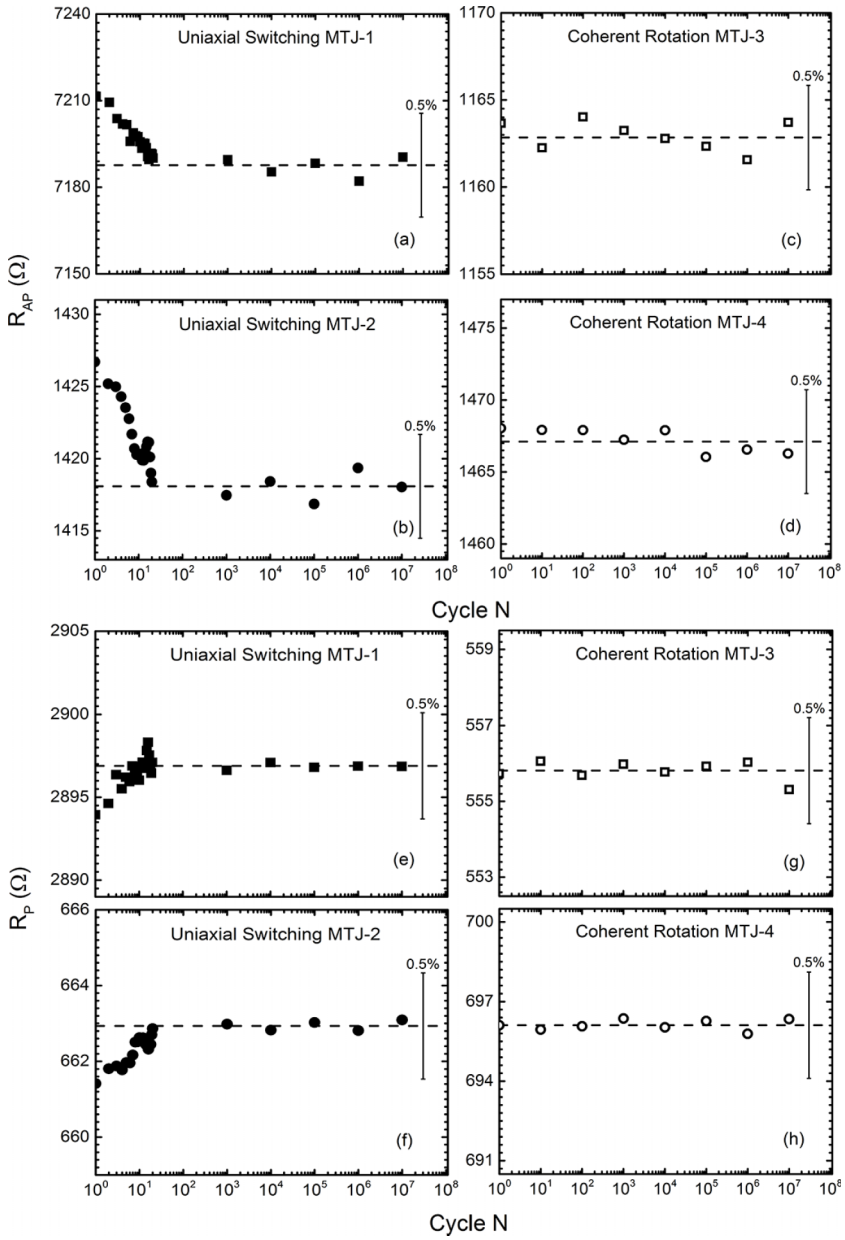

FIG. 4. R_{AP} and R_P values as functions of magnetic cycling number N for sample MTJ-1 (a)(e) and MTJ-2 (b)(f) undergoing uniaxial magnetic switching, and for sample MTJ-3 (c)(g) and MTJ-4 (d)(h) undergoing coherent rotation.

the magnetization state of the hard layer becomes less uniform or even disintegrates logarithmically during long-term endurance.[8–12] This magnetic decay leads to a decrease in $R_{AP}(N)$, and a corresponding increase in $R_P(N)$, as observed in Fig. 4. In other words, any deviation from an (anti)parallel orientation in the mutual spin alignments would converge $R_{AP}(N)$ and $R_P(N)$, and reduce the TMR value. The fact that the TMR decays less than 2% during only the short "training period" demonstrates the excellent magnetic stability of the MTJ structure used in our study. In our SAF pinned layer, $Co_{50}Fe_{50}(2)$/IrMn(15)/$Co_{50}Fe_{50}(2)$/Ru(0.8)/ $Co_{40}Fe_{40}B_{20}(3)$, the $Co_{40}Fe_{40}B_{20}(3)$ is antiferromagnetically coupled to $Co_{50}Fe_{50}(2)$ through a thin Ru(0.8) layer. The SAF layer is further exchange-biased by the antiferromagnetic IrMn(15) layer. Magnetic thermal annealing under 0.45 T sets the exchange bias at the IrMn/CoFe interface. In addition, it ensures the magnetic uniformity of the SAF hard layer. Without the magnetic thermal annealing, any local magnetic

disorders within the CoFe layer can induce magnetic disorders onto the CoFeB layer through Ru. Magnetic annealing brings about a uniform magnetization state of the CoFe layer and the CoFeB via a strong antiferromagnetic coupling via Ru. The stray fields from the free layer have canceling effects (*push and pull*) on the SAF *bi-layer*. This is the reason why SAF layers are such a stable magnetic structure with regard to magnetic fatigue.

The initial decrease in TMR during the "training period" indicates that there exist some minority non-equilibrium spin configurations in the hard layer. These minority spin components can be easily cured with 20 uniaxial switching cycles. Therefore, it is imperative to "train" any commercial MTJ devices before use. Fortunately, only a very quick "training" can accomplish the task. This compares most favorably to other types of solid-state magnetoresistance sensors that require periodic "trainings" using large electric current pulses to eliminate magnetic domain randomization caused by fatigue. In earlier studies, various types of MTJ layer structures and switching modes have been suggested to mitigate the effect of magnetic instability.[8,12,17,19] The exchange-biased SAF hard layer studied here is simple to implement and possesses high magnetic stability.

Our study on the magnetic stability is on MTJs with a memory configuration in which the easy axis of the free layer is parallel to the pinning direction of the pinned layer. In the coherent rotation mode, the free layer magnetization vector rotates continuously. This mode encompasses both the memory configuration and the sensor configuration, in which the magnetization vectors of the free and the pinned layers are perpendicular to each other. Our results are, therefore, relevant to MTJs with the sensor configuration.

The aspect ratio of our MTJ free layer is 1.8. In some MTJ sensors, the aspect ratio may be larger (e.g., 10). In general, the stability of MTJ sensors with larger aspect ratios tend to be higher, because the stronger demagnetizating effect tends to keep the free layer in the magnetic single domain state.

In summary, we have achieved long-term magnetic stability in MgO-based MTJs. During uniaxial magnetic switching of the free layer, TMR decreases less than 1.7 % during the first 20 cycles and becomes stabilized thereafter up to 10^7 cycles, which is the limit of our endurance test. No variation in TMR within experimental error is observed during coherent rotations of the free layer. The superior stability is a result of the hard layer structure based on an exchange-biased synthetic antiferromagnetic coupling. The hard layer structure significantly mitigates the strong demagnetization effect from the stray fields generated by the domain walls within the free layer. Coercivity of the free layer is unchanged within errors up to 10^7 cycles. After only 20 cycles of "training", the MTJs can perform long-term operation without any loss in key parameters. The MTJ layered structure used in this study is magnetically durable for both magnetic sensing and MRAM applications.

ACKNOWLEDGMENTS

This work was supported by National Science Foundation through Grant No. DMR-1307056 and Nanoelectronics Research Initiative (NRI) through the Institute for Nanoelectronics Discovery and Exploration (INDEX).

[1] J. Moodera, L. Kinder, T. Wong, and R. Meservey, "Large magnetoresistance at room temperature in ferromagnetic thin film tunnel junctions," Phys. Rev. Lett. **74**, 3273 (1995).
[2] T. Miyazaki and N. Tezuka, "Giant magnetic tunneling effect in Fe/Al2O3/Fe junction," J. Magn. Magn. Mater. **139**, L231 (1995).
[3] S.S.P. Parkin, C. Kaiser, A. Panchula, P.M. Rice, B. Hughes, M. Samant, and S. Yang, "Giant tunnelling magnetoresistance at room temperature with MgO (100) tunnel barriers," Nature Materials **3**, 862 (2004).
[4] S. Yuasa, T. Nagahama, A. Fukushima, Y. Suzuki, and K. Ando, "Giant room-temperature magnetoresistance in single-crystal Fe/MgO/Fe magnetic tunnel junctions," Nature Materials **3**, 868 (2004).
[5] Gang Xiao, "Magnetoresistive sensors based on magnetic tunneling junctions," in *Handbook of Spin Transport and Magnetism*, edited by E. Tsymbal and I. Zutic (CRC Press, Taylor & Francis Group, Boca Raton, 2012), Chap. 34.
[6] See reviews in IBM Journal of Research and Development, January 2006.
[7] S.A. Wolf, D. D. Awschalom, R. A. Buhrman, J. M. Daughton, S. von Molnar, M. L. Roukes, A. Y. Chtchelkanova, and D. M. Treger, "Spintronics: a spin-based electronics vision for the future," Science **294**, 1488 (2001).
[8] S. Gider, B.-U. Runge, A. C. Marley, and S. S. P. Parkin, "The magnetic stability of spin-dependent tunneling devices," Science **281**, 797 (1998).

[9] M. R. McCartney, R. E. Dunin-Borkowski, M. R. Scheinfein, D. J. Smith, S. Gider, and S. S. P. Parkin, "Origin of magentization decay in spin-dependent tunneling junctions," Science **286**, 1337 (1999).
[10] L. Thomas, J. Lüning, A. Scholl, F. Nolting, S. Anders, J. Stöhr, and S. S. P. Parkin, "Oscillatory decay of magnetization induced by domain-wall stray fields," Phys. Rev. Lett. **84**, 3462 (2000).
[11] L. Thomas, M. G. Samant, and S. S. P. Parkin, "Domain-wall induced coupling between ferromagnetic layers," Phys. Rev. Lett. **84**, 1816 (2000).
[12] J. Schmalhorst, H. Brückl, G. Reiss, R. Kinder, G. Gieres, and J. Wecker, "Switching stability of magnetic tunnel junctions with an artificial antiferromagnet," Appl. Phys. Lett. **77**, 3456 (2000).
[13] O. Lenoble, M. Hehn, D. Lacour, A. Schuhl, D. Hrabovsky, J. F. Bobo, B. Diouf, and A. R. Fert, "Domain duplication in magnetic tunnel junctions studied by Kerr microscopy," Phys. Rev. B **63**, 052409 (2001).
[14] B. D. Schrag, A. Anguelouch, S. Ingvarsson, Gang Xiao, Yu Lu, P. L. Trouilloud, A. Gupta, R. A. Wanner, W. J. Gallagher, P. M. Rice, and S. S. P. Parkin, "Neel 'orange-peel' coupling in magnetic tunneling junction devices," Appl. Phys. Lett. **77**, 2373 (2000).
[15] A. Inomata, J. S. Jiang, C.-Y. You, J. E. Pearson, and S. D. Bader, "Magnetic stability of novel exchange coupled systems," Journal of Vacuum Science & Technology A **18**, 1269 (2000).
[16] J. S. Jiang, A. Inomata, C.-Y. You, J. E. Pearson, and S. D. Bader, "Magnetic stability in exchange-spring and exchange-bias systems after multiple switching cycles," J. Appl. Phys. **89**, 6817 (2001).
[17] Chun-Yeol You and S. D. Bader, "Enhancement of switching stability of tunneling magnetoresistance systems with artificial ferrimagnets," J. Appl. Phys. **92**, 3886 (2002).
[18] Hyun Soon Park, J. Spencer Baskin, and Ahmed H. Zewail, "4D Lorentz electron microscopy imaging: magnetic domain wall nucleation, reversal, and wave velocity," Nano Lett. **10**, 3796 (2010).
[19] P. Warin, T. N. Tran Thi, P. dePerson, M. Jamet, C. Beigne, and Y. Samson, "Hard layer demagnetization by soft layer cycling in a MgO-based perpendicular magnetic tunnel junction," J. Magn. Magn. Mater. **323**, 217 (2011).
[20] A. Cousins, G. L. Balalis, S. K. Thompson, D. Forero Morales, A. Mohtar, A. B. Wedding, and B. Thierry, "Novel handheld magnetometer probe based on magnetic tunneling junction sensors for intraoperative sentinel Lymph node identification," Scientific Reports **5**, 10842 (2015).
[21] M. L. Chan, G. Jaramillo, K.R. Hristova, and D.A. Horsley, "Magnetic scanometric DNA microarray detection of methyl tertiary butyl ether degrading bacteria for environmental monitoring," Biosensors and Bioelectronics **26**, 2060 (2011).
[22] E. A. Lima, A. C. Bruno, H. R. Carvalho, and B. P. Weiss, "Scanning magnetic tunnel junction microscope for high-resolution imaging of remanent magnetization fields," Measurement Science and Technology **25**, 105401 (2014).
[23] G. Jaramillo, M. L. Chan, J.O. Milewski, and R.D. Horsley, "Ferrite Scanning Microscope Based on Magnetic Tunnel Junction Sensor Ferrite Scanning Microscope Based on Magnetic Tunnel Junction Sensor," IEEE Trans. Magnetics **48**, 3677 (2015).
[24] H. Maehara *et al.*, "High Q factor over 3000 due to out-of-plane precession in nano-contact spin-torque oscillator based on magnetic tunnel junctions," Appl. Phys. EXPRESS **7**, 023003 (2014).
[25] D. W. Guo, F. A. Cardoso, R. Ferreira, E. Paz, S. Cardoso, and P. P. Freitas, "MgO-based magnetic tunnel junction sensors array for non-destructive testing applications," J. Appl. Phys. **115**, 17E513 (2014).
[26] J. Sánchez, D. Ramírez, S.I. Ravelo, A. Lopes, S. Cardoso, R. Ferreira, and P.P. Freitas, "Electrical characterization of a magnetic tunnel junction current sensor for industrial applications," IEEE Trans. Magn. **48**, 2823 (2012).
[27] S. H. Liou, X. L. Yin, S. E. Russek, R. Heindl, F. C. S. Da Silva, J. Moreland, D. P. Pappas, L. Yuan, and J. Shen, "Picotesla magnetic sensors for low-frequency applications," IEEE Trans. Magn. **47**, 3740 (2011).